INTERNATIONAL JOURNAL OF COMPUTERS COMMUNICATIONS & CONTROL
Online ISSN 1841-9844, ISSN-L 1841-9836, Volume: 20, Issue: 5, Month: October, Year: 2025
Article Number: 6829, https://doi.org/10.15837/ijccc.2025.5.6829

Evaluating the Maximum Region for Parametric Model Uncertainties in Variable-Oriented Photovoltaic Systems

D. Bancila, S. Colbu, D. Popescu

Daniel - Marian Bancila
Dept.of Automatic Control and Systems Engineering,
National University of Science and Technology POLITEHNICA Bucharest, Romania
*Corresponding author: daniel.bancila@stud.acs.upb.ro

Stefania - Cristiana Colbu
Dept.of Automatic Control and Systems Engineering,
National University of Science and Technology POLITEHNICA Bucharest, Romania
stefania.colbu@stud.acs.upb.ro

Dumitru Popescu
Dept.of Automatic Control and Systems Engineering,
National University of Science and Technology POLITEHNICA Bucharest, Romania
dumitru.popescu@acse.pub.ro

Abstract

Renewable energy has been a worldwide subject of interest in the last decades, because of the need to reduce greenhouse gas emissions. Solar is among the most widespread energy resources as it has almost limitless installation possibilities on Earth's surface. Photovoltaic panels play a key role in the energy industry, having a dynamically evolving chemical structure of the cell and being implemented in many applications within various weather conditions. This paper will focus on introducing and analyzing an optimal control strategy for variable-oriented photovoltaic systems to address the issue of suboptimal generation. In contrast with the traditional Maximum Power Point Tracking (MPPT) approaches, a stability analysis will be performed and parametric model uncertainties will be introduced to emulate the real-world variable conditions, such as temperature and irradiance changes. These uncertainties will help determine the maximum region for which the control strategy still keeps the best performances, regarding reference tracking and regulation. The novelty of the paper comes from introducing in the photovoltaic control and optimization field, the approach of delimiting the parametric uncertainty margins, for which a designed Linear Quadratic Regulator (LQR) controller will keep the stability and performances, which was not previously addressed in this field. Accordingly, it will be shown that a robust controller can guarantee maximum power at output even though the model of the system evolved influenced by environmental factors, degradation of the system's components or another system's abnormal behavior. In this paper, it will be also introduced a series of simulation results, that will emphasize the stabilized system evolution for various uncertainties within the computed maximum stability margins. The simulation findings indicate that the implemented robust LQR will offer similar response time, without oscillations and, implicitly, similar performances for the entire family of parametric uncertainties added to the initial system. In other words, the approach can offer a cost-effective solution for sustainable large-scale energy production.

Keywords: uncertainty region, optimal control, stability, renewable energy.

1 Introduction

In the field of renewable energy the electrical power extracted from the sun represents 7% of the energy produced from all renewable sources in the European Union (EU)[27]. One-seventh of the world total energy approximately since 2020 is produced now from renewable resources [20]. Nevertheless, the electrical power extracted from the solar irradiance has been the fastest-growing energy in the EU, and until 2030 it is aimed to have 600 GW installed power, from 41.4 GW as it was in 2022 [19]. To this scope can contribute on one hand, the improvement of the photovoltaic cell in the manufacturing process, and on the other hand, the control strategy used to maximize the output power, delivered to the end customer [14].

In the pursuit of optimizing photovoltaic system performance, MPPT algorithms play a crucial role in establishing that solar panels operate at their maximum efficiency. Extensive literature has documented various MPPT techniques, highlighting their effectiveness in different environmental conditions and their continuous evolution to improve energy production [6, 7, 24]. The focus of the current paper will be to introduce an innovative approach in this field, consisting in an optimal controller designed starting from the state representation of the photovoltaic system and introducing parametric uncertainties to emulate the real world continuously changing conditions.

Photovoltaic tracking and power systems have evolved during the past decades and nowadays they consist in: one or two DC/DC motors used to tilt the panel horizontally and vertically, the panel formed from multiple photovoltaic cells, a power transducer and one or many controllers. It will be studied the case with one motor used to tilt the panel for changing its altitude angle, in the vertical plane. This is because the generated power of tilt panels at irradiance peak hours can be upper with 40% , compared to fixed panels. And the average percentage of enhancement compared to fixed panels is 31% for single motor and 34.7% for dual motor [2]. For the current study it was chosen a single axis motor, for the performance linked to its cost and the consumed energy from the system.

For finding the optimal tilt angle of a photovoltaic panel, various approaches have been tried in the literature, some proposed a searching algorithm for iterating values from 0° to 60°, with a step of 1° [10]. However, this method is based on scenario analysis and can lead to computational complexity, making it unsuitable for real-time applications. Other researchers have employed a Support Vector Machine(SVM) model in combination with a data system for geographical information to demonstrate that the PV potential can be predicted with high accuracy [4]. Nevertheless, the conclusions of this study are applied exclusively in specific locations in Switzerland. To apply these results worldwide, certain parameters of the model may require to be tuned to consider different regions and their unique environmental factors. Additionally, the energy consumption of the area where the panel is installed may need to have implemented optimal approaches for electricity usage, when the energy production is constrained as studied in [16]. Moreover, the power coming from the photovoltaic system needs to be distributed through a network to reach the end user, and this network needs to be designed and maintained to withstand a wide range of faults as presented in [13].

The proposed approach consists of an optimal controller designed for the model of the photovoltaic system, giving the advantage of the possibility to be implementable on a controller linked to the physical system, which can use limited computational resources. One important challenge in control under PV systems is the uncertainty in the system's parameters. In this regard, a robust LQR control method will be proposed to take into account the variations in system parameters. With this, the stability and the optimal performance will be maintained under the parametric uncertainties that will be considered, since the analyzed system is influenced by the environmental temperature, the solar irradiance and the shading.

The paper is structured in the following sections: The second part includes details about the related work on LQR control strategy applied for PV configurations; the third section defines the methodology of research, including the overall theoretical framework, the modeling of the dynamics for the photovoltaic system, the design of the optimal controller and the evaluation of the maximum region related to the considered parametric uncertainties, taking into account the stability bounds; the fourth section consists in simulated results and analysis; the fifth section offers the conclusions and the future directions of the research.

2 Related works

The introduction of the photovoltaic system in energy grids is one of the core means of achieving alternative or sustainable energy solutions. Ensuring the efficiency and stability of these systems is crucial for their widespread adoption. A very effective method to develop those aspects is by applying Linear Quadratic Regulator control. LQR control applied in PV systems can operate the dynamic behavior of power converters effectively or of the motors used to move the panels, thus guaranteeing MPPT.

A few works have outlined the potentiality of LQR control for different PV system configurations. For instance, in [17], the authors combined LQR with fuzzy control in a grid-connected PV system, that depicted improved stability and disturbance rejection. This study involved a system with a Buck-Boost DC-DC converter, a DC-AC inverter and four 250 W PV panels. The control strategy included a fuzzy-based incremental conductance (INC) algorithm for MPPT, a hybrid fuzzy PI controller for DC-link voltage regulation, and an LQR for current control to the grid [17]. The hybrid approach demonstrated quick settling times and robust performance under various weather conditions, outperforming previous methods. The LQR algorithm proved to be more resistant to sudden disturbances, with simulation results showing the system's ability to handle variations in weather parameters.

Similarly, in [3], an LQR-based MPPT approach was proposed for standalone PV systems. This method achieved higher tracking speed and efficiency compared to traditional Perturb and Observe (P&O) technique. The LQR-based MPPT method was validated through simulations and experimental results, showing superior tracking speed and efficiency under varying irradiance conditions. The benefits of this method include faster tracking ability, transmission of the maximum deliverable power, and reduction in complexity [3]. The improved performance was confirmed by deploying this method to a dSPACE controller, highlighting the method's effectiveness in real-world applications.

3 Methods

3.1 Overall theoretical framework

The global theoretical framework consists of a specific strategy introduced to increase the efficiency of a variable-oriented solar system. This framework was divided into multiple major components:

1. In the current approach, the first step was to model the photovoltaic system, based on the DC motor, the photovoltaic panel and power transducer dynamics. This mathematical model of the system was built by capturing the relationship between the electrical output and the irradiance. Afterwards, the initial transfer function of the system was transformed in a state-space representation. This representation was adopted to analyze the dynamic behavior of the plant and is essential for the design of the optimal control strategy.

2. As a second step, an optimal controller was designed to maximize the power output of the variable-oriented PV system. The controller computed based on LQR aimed to secure that the PV panel operated at its maximum power point. The design process included defining the cost function, deriving the control law and implementing the controller.

3. In order to maintain the performance under variable weather conditions, the study examined the maximum uncertainty region for parametric model uncertainties. This involved analyzing how variations in model parameters affect the system performance and stability. Robust control techniques were implemented to ensure that the controller can effectively handle these uncertainties.

4. A thorough stability analysis is conducted to insure the system remains stable under specific operating conditions. This included both theoretical analysis and simulation studies of the stability margins based on the Structured Singular Value Analysis (μ-Analysis). This guaranteed that the system can withstand environmental variations and continue to operate reliably.

The theoretical framework provided a structured approach to the configuration and analysis of control systems for PV panels. By integrating mathematical modeling, optimal control design, uncertainty analysis, and stability validation, the framework guarantees that the system can achieve maximum power generation and maintain a stable operation under varying conditions.

3.2 Models & dynamics of the photovoltaic system

The dynamics of a variable-oriented photovoltaic system are computed considering the following components: the DC motor, the photovoltaic panel and the power transducer.

The entire photovoltaic system's transfer function is defined by connecting all the sub-systems in series [5]:

$$H_F(s) = H_m(s) \cdot H_{pv}(s) \cdot H_T(s) \tag{1}$$

3.2.1 Mathematical model of the DC motor

The DC motor defines the movement of the photovoltaic panel in order to orient it towards the sun to generate the maximum power measured by the transducer.

The MPP is attained by changing the position of the system, by tilting or rotating the photovoltaic panel using a DC motor. The electrical diagram of the studied DC motor can be found in Figure 1:

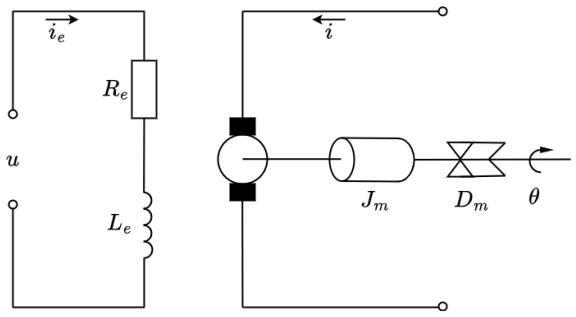

Figure 1: Electrical Diagram: DC motor

The DC motor can be mathematically modeled based on the hypothesis of linearization around an operating point [1]:

$$\begin{cases} u(t) & = L_e \frac{di_e(t)}{dt} + R_e i_e(t) + e_e(t) \\ K_m i_e(t) & = J_m \frac{d^2\theta(t)}{dt^2} + D_m \frac{d\theta(t)}{dt} \end{cases} \tag{2}$$

The existing i current coming from an independent source (that can be a fraction of the panel production) feeds the motor defined by the resistance R_e, and the inductance L_e in the excitation circuit. J_m represents the moment of inertia, D_m stands for the coefficient of viscous friction, and the voltage u is applied at the terminals of the excitation circuit, with the current i_e flowing through this circuit. Moreover, the expression of the electromotive voltage is considered according to

$$e(t) = K_e \cdot \frac{d\theta(t)}{dt}$$

(K_e, where K_e is the electrical constant).

The angular position θ of the shaft represents the motor's output quantity. The angular velocity is represented by $\dot{\theta} = \frac{d\theta}{dt}$ and the angular acceleration is $\ddot{\theta} = \frac{d^2\theta}{dt^2}$. Also, K_m is a proportionality factor relating current to torque.

The balance between the motor torque $K_m i_e(t)$ and the torques due to acceleration and viscous friction is expressed in the first equation. The second equation arises from applying Kirchhoff's Law to the excitation circuit.

In addition, the angular speed can be expressed based on the tilt angle (α) of the panel through the following expression:

$$\Omega_m(s) = s \cdot \alpha(s) \tag{3}$$

Considering the angular speed denoted by Ω_m and by applying the Laplace transform, the system described in the Equation (2) becomes:

$$\begin{cases} U(s) & = sL_eI_e(s) + R_eI_e(t) + K_e\Omega_m(s) \\ sJ_m\Omega_m(s) & = K_mI_e(s) - D_m\Omega_m(s) \end{cases} \tag{4}$$

In these terms, the DC motor's transfer function can be defined as:

$$H_m(s) = \frac{\alpha(s)}{U(s)} = \frac{1}{s} \frac{K_m}{L_eJ_ms^2 + (R_eJ_m + L_eD_m)\, s + K_eK_m + R_eD_m} \tag{5}$$

Based on the panel size, environmental conditions, and the available budget, various types of DC motors can be selected. For larger panels, a motor with a high torque constant K_m should be considered. If a rapid rotation of the panel is desired, the nominal speed ω_{mn} should be high. In terms of power supply, in such situations, values of $12V$ or $24V$ are used.

3.2.2 Mathematical model of the photovoltaic panel

The transfer function of a photovoltaic panel can be defined based on the electronic behavior of its components. In this case, the focus will be on the generated power - $\mathcal{P}_{gen}$, influenced by the panel's tilt angle - $\alpha\,[rad]$. Thus, we can start from the angle-dependent relationship and compute the maximum power at the optimal tilt angle.

$$\mathcal{P}_{gen} = \mathcal{P}_{max}\mathcal{F}(\alpha) \tag{6}$$

The Earth's axis has an inclination of approximately 23.45° relative to the orbital plane around the sun [9]. This inclination influences temperature, seasons, day length, air and water circulation, but most importantly, it affects the intensity of solar irradiance, which plays a crucial role in photovoltaic energy production. The angle formed from a normal to the Earth's surface and the sun's rays, known as zenith angle θ, can be calculated as follows: $\cos\theta = \sin\phi \cdot \sin\delta + \cos\phi \cdot \cos\delta\cos\omega$, where ϕ represents the location's latitude, and ω is the solar hour angle indicated by shading [23]. The sun declination δ is the angle between a plane perpendicular to a line connecting the sun to Earth, and the Earth's axis. Sun's position is indicated by the azimuth angle γ, and all the angles can be seen in Figure 2 [23].

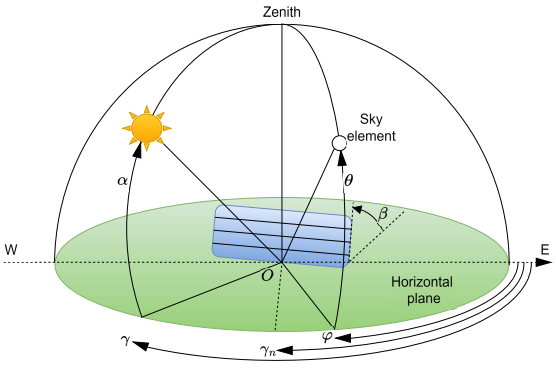

Figure 2: The main angles between the photovoltaic panel and the solar plane[23]

At sunset or sunrise, the sun is on the horizon. Therefore, the corresponding angle for sunset/sunrise can be determined based on:

$$\omega_{rs,ap} = arccos\,(-tan\ \phi \cdot tan\delta\ ) \tag{7}$$

The intensity of the sunlight on a tilted plane can be calculated using the formula [23]:

$$R_b = \frac{\cos(\phi - \beta)\cos\delta\sin\omega_{ap} + \omega_{ap}\sin(\phi - \beta)\sin\delta}{\cos\phi\cos\delta\sin\omega_{ap} + \omega_{ap}\sin\phi\sin\delta} \tag{8}$$

The tilt angle of the system that corresponds to the point of maximum power generation is strongly linked with the solar radiation $\mathcal{H}_{\alpha G}$, that can be computed based on the following sum [12]:

$$\mathcal{H}_{\alpha G} = \mathcal{H}_{\alpha B} + \mathcal{H}_{\alpha D} + \mathcal{H}_{\alpha R} \tag{9}$$

, where $\mathcal{H}_{\alpha B}\left[\frac{Wh}{m^2}\right]$ represents the direct normal radiation on a flat surface, $\mathcal{H}_{\alpha D}\left[\frac{Wh}{m^2}\right]$ corresponds to the diffuse radiation from the sky on a plane, and $\mathcal{H}_{\alpha R}\left[\frac{Wh}{m^2}\right]$ denotes the reflected radiation from the ground on a flat surface.

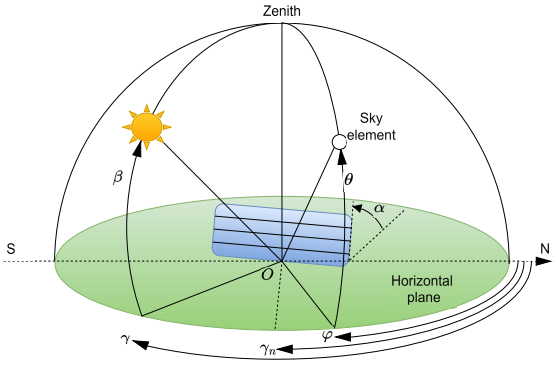

Figure 3: The angle of tilt for the solar plant

In the following equations the $\mathcal{H}_{\alpha B}$ and $\mathcal{H}_{\alpha R}$ will be expressed as [12]:

$$\mathcal{H}_{\alpha B} = \cos\psi \mathcal{H}_{nB} \tag{10}$$

$$\mathcal{H}_{nB} = \frac{\mathcal{H}_{hB}}{\sin\beta} \tag{11}$$

$$\cos\psi = \cos\alpha \sin\beta + \cos\beta \sin\alpha \cos|\gamma - \gamma_n| \tag{12}$$

$$\mathcal{H}_{\alpha R} = \rho \mathcal{H}_{hG} \frac{1 - \cos\alpha}{2} \tag{13}$$

where $\mathcal{H}_{nB}\left[\frac{Wh}{m^2}\right]$ represents the direct normal radiation on a flat surface, $\mathcal{H}_{hB}\left[\frac{Wh}{m^2}\right]$ the incident radiation on a horizontal surface, $\mathcal{H}_{hG}\left[\frac{Wh}{m^2}\right]$ the global radiation in a horizontal plane, $\psi[rad]$ is the incidence angle, $\beta[rad]$ is known as solar altitude, $\gamma[rad]$ the solar azimuth, $\gamma_n[rad]$ the normal azimuth angle, and ρ is the ground reflectivity [12].

The radiation on a flat surface originating from a limited section of the sky ($\delta\mathcal{H}$) is computed based [12]:

$$\delta\mathcal{H} = \delta\omega R_{\theta\phi} \cos\sigma \tag{14}$$

$$\delta\omega = \delta\theta \cos\theta \delta\phi \tag{15}$$

$$\cos\sigma = \cos\alpha \sin\theta + \cos\theta \cos\phi \sin\alpha \tag{16}$$

, where $R_{\theta\phi}\left[W/m^2 sr\right]$ is the radiation received from an element of the sky located at altitude θ and azimuth ϕ, $\omega_{solid}[sr]$ is the solid angle, and $\sigma[rad]$ is the angle formed between the element from the sky and the normal to the surface [12].

By applying a double integral on the surface, the $\mathcal{H}_{\alpha D}$ is defined as in [12]:

$$\mathcal{H}_{\alpha D} = R_{\theta\phi} \cos\theta \left(\cos\alpha \sin\theta + \cos\theta \cos\phi \sin\alpha\right) d\phi d\theta \tag{17}$$

If the diffuse component of the sky is divided into n_a angular zones, the Equation (17) can be numerically computed as follows:

$$\mathcal{H}_{\alpha D} = \Sigma_{i=1}^{n_a} \cos\sigma_i R_i \omega_{solid_i} \tag{18}$$

Taking into account these equations and the solar irradiance intensity at various times of the day and during different solar exposure intervals, an ideal average tilt angle for the panel for the specific area need to be computed.

When it comes to the dynamics of how the power at the output of the photovoltaic panel changes based on its tilt angle, this variation is significantly faster than the dynamic response of the motor. Therefore, the photovoltaic panel can be modeled using a gain, assuming that the panel's tilt angle remains within the average range.

This gain depends mainly on the transfer gain from the angular momentum generated by the motor to tilt angle of the panel, denoted as $\alpha(s) = \frac{1}{s} \cdot \omega_m(s)$ [5]:

$$K_\alpha = \frac{\frac{\Delta\alpha}{\alpha_0}}{\frac{\Delta\omega_m}{\omega_{m0}}} \tag{19}$$

Starting from the fact that the motor can achieve an inclination between 0^o and the average angle value, α_0 can be obtained from the static linear characteristic.

$$\alpha_0 = \frac{\omega_{m0} - \omega_{mmin}}{\omega_{mmax} - \omega_{mmin}} \left(\alpha_{UI_{max}} - \alpha_{UI_{min}}\right) + \alpha_{UI_{min}} \tag{20}$$

For a minimum power output $\mathcal{P}_{gen_0}$ imposed, under which the generated power value should not decrease, the transfer function becomes:

$$H_{pv}(s) = K_{pv} = \frac{\frac{\Delta\mathcal{P}_{gen}}{\mathcal{P}_{gen_0}}}{\frac{\Delta\alpha}{\alpha_0}} \tag{21}$$

3.2.3 Mathematical model of the power transducer

The power transducer defines also rapid dynamics, relative to the dynamics of the DC motor. Therefore, it can be modeled entirely through a gain.

The current $\mathcal{I}$ is considered to be the output in the standardized $4 - 20\ mA$ signal, and $\mathcal{I}_0$ is derived from the static characteristic [5].

$$\mathcal{I}_0 = \frac{\mathcal{P}_{gen_0} - \mathcal{P}_{gen_{min}}}{\mathcal{P}_{gen_{max}} - \mathcal{P}_{gen_{min}}} \left(\mathcal{I}_{UI_{max}} - \mathcal{I}_{UI_{min}}\right) + \mathcal{I}_{UI_{min}} \tag{22}$$

The transfer function of the transducer becomes:

$$H_T(s) = K_T = \frac{\frac{\Delta\mathcal{I}}{\mathcal{I}_0}}{\frac{\Delta\mathcal{P}_{gen}}{\mathcal{P}_{gen_0}}} \tag{23}$$

3.2.4 State-space representation of the variable-oriented photovoltaic system

In state-space representation, a system is defined based on differential equations that encapsulate state variables with time-varying values. These variables depend on their previous values as well as the system's inputs and outputs [21]. Simultaneously, the state variables, in turn, influence the output value.

The relationship that describes the state-space representation for a linear system is given in [21]:

$$\begin{cases} \dot{x}(t) = \mathcal{A}x(t) + \mathcal{B}u(t) \\ y(t) = \mathcal{C}x(t) + \mathcal{D}u(t) \end{cases} \tag{24}$$

The vector representing the system state at various time instances t is denoted by $x\,(t) \in \mathbb{R}^n$. In this case, n represents the number of independent state variables. The vector representing the system

outputs at various time instances t is denoted by $y(t) \in \mathbb{R}^q$, where q is the number of independent system outputs. The vector corresponding to the control input is denoted by $u(t) \in \mathbb{R}^p$, with p representing the number of inputs to the process. The state matrix is denoted by $\mathcal{A} \in \mathbb{R}^{n \times n}$. The matrix corresponding to the input is denoted by $\mathcal{B} \in \mathbb{R}^{n \times p}$. The output matrix is denoted by $\mathcal{C} \in \mathbb{R}^{q \times n}$. The feedforward matrix is denoted by $\mathcal{D} \in \mathbb{R}^{q \times p}$.

The relationship between the state-space system and its representation as a transfer function is expressed as follows, knowing that $\mathbb{I} \in \mathbb{R}^{nxn}$ is the identity matrix [21]:

$$H_F(s) = \mathcal{C}\left(s\mathbb{I} - \mathcal{A}\right)^{-1}\mathcal{B} + \mathcal{D} \tag{25}$$

To assess whether a feedback control law can be computed or a regulator with an integrated state estimator can be designed, it is suggested to build the controllability matrix $\mathbf{C}_F = [\mathcal{B}\ \mathcal{A}\mathcal{B} \cdots \mathcal{A}^{n-1}\mathcal{B}]$ and the observability matrix $\mathbf{O}_F = \begin{bmatrix} \mathcal{C} \\ \mathcal{C}\mathcal{A} \\ \vdots \\ \mathcal{C}\mathcal{A}^{n-1} \end{bmatrix}$ [25].

3.3 Optimal control design strategy

Based on the fact that the previously presented state-space representation has been demonstrated to be minimal, a state feedback controller will be designed.

Starting from the representation in the Equation (24):

$$\begin{cases} \dot{x}(t) & = \mathcal{A}x(t) + \mathcal{B}u(t), \\ x(t_0) & = x_0 \end{cases} \tag{26}$$

, with the state vector x assumed to be measurable for state feedback control. Furthermore, the pair $(\mathcal{A}, \mathcal{B})$ is assumed to be stabilizable (i.e. there exists a matrix $\mathcal{K}$ such the matrix $(\mathcal{A} - \mathcal{B}\mathcal{K})$ is stable in the sense of Hurwitz stability).

To achieve both tracking and disturbances rejection performances in the state-space, a LQR can be applied. Implementing this regulator requires minimizing the criterion that penalizes deviations in the control input u and in the state x [8]. This process results in the computation of a stabilizing state-feedback control law [8]:

$$\mathcal{L} = \int_0^\infty \left(x^T(t)\,\mathcal{Q}x(t) + u^T(t)\,\mathcal{R}u(t)\right) dt \tag{27}$$

where the matrices $\mathcal{Q}$ and $\mathcal{R}$ are symmetric and positive definite.

The previously selected matrices are joined by matrix $\mathcal{K}_{LQR}$, which is defined as the gain matrix corresponding to the optimal command:

$$\begin{cases} u(t) = -\mathcal{K}_{LQR} \cdot x(t) \\ \mathcal{K}_{LQR} = \mathcal{R}^{-1}\mathcal{S}\mathcal{B}^T \end{cases} \tag{28}$$

$\mathcal{S}$ is determined as the solution to the algebraic Riccati equation [8] for the LQR regulator:

$$\mathcal{S}\mathcal{A} + \mathcal{A}^T\mathcal{S} - \mathcal{S}\mathcal{B}\mathcal{R}^{-1}\mathcal{B}^T\mathcal{S} + \mathcal{Q} = 0 \tag{29}$$

Figure 4 ilustrates the closed-loop system diagram:

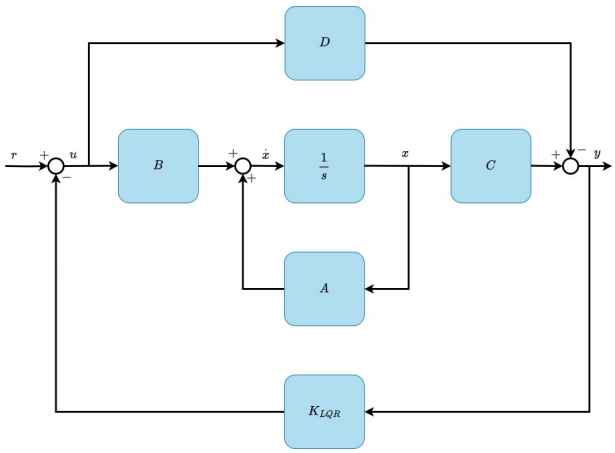

Figure 4: Closed-loop state-space representation of the system

3.4 Evaluation of the maximum uncertainty region

3.4.1 Robust LQR - Parametric uncertainties

The state feedback is stabilizing the system, meaning that $\mathcal{A}-\mathcal{B}\mathcal{K}_{LQR}$ is stable in a Hurwitz sense (all the roots of the defined polynomial are in the left half-plane) [18] and the criterion $\mathcal{L}(x_0)$ is defined as a minimal one:

$$\mathcal{L}(x_0) = x_0^T \mathcal{S} x_0 \tag{30}$$

for all bounded initial conditions x_0. Additionally, $V(x) = x^T \mathcal{S} x$ is a Lyapunov function associated to the considered system having the properties [15]:

$$\begin{cases} V(x) > 0, for \quad x \neq 0 \\ \dot{V}(x) = -x^T \left(\mathcal{Q} + \mathcal{K}_{LQR}^T \mathcal{R} \mathcal{K}_{LQR} \right) x < 0, \text{for } x \neq 0 \end{cases} \tag{31}$$

All the uncertainties that can affect the photovoltaic tracking and power system are parametric, because the irradiance, the wind, the temperature, and the shading of the panel have models that can be expressed in a parametric mathematical model. Consequently, in the state representation the parametric uncertainties were considered:

$$\begin{cases} \dot{x}(t) = (\mathcal{A} + \Delta\mathcal{A}(t))\, x(t) + (\mathcal{B} + \Delta\mathcal{B}(t))\, u(t) \\ y(t) = \mathcal{C} x(t) + \mathcal{D} u(t) \end{cases} \tag{32}$$

The output $y(t)$ depends on the command $u(t)$ only through the state variables $x(t)$, this means that $\mathcal{D} = 0$ is considered. The pair $(\Delta\mathcal{A}(t), \Delta\mathcal{B}(t))$ indicates parametric uncertainties affecting the pair of matrix $(\mathcal{A}, \mathcal{B})$, defined in the Equation (24).

The transfer function including the uncertainties becomes:

$$H_F(s) = \mathcal{C}(s\mathbb{I}_n - \mathcal{A} - \Delta\mathcal{A})^{-1}(\Delta\mathcal{B} - \mathcal{B}) \tag{33}$$

It is needed to introduce the uncertainty domain, which defines the region where the matrix can vary and the stability of the system can still be valid [15]:

$$D_u = \left\{ (\Delta\mathcal{A}(t), \Delta\mathcal{B}(t)) \,\|\, \Delta\mathcal{A}^T(t)\mathcal{A}(t) \leq \gamma_{\mathcal{A}} \mathcal{Q}_0, \Delta\mathcal{B}(t) \leq \gamma_{\mathcal{B}} \mathcal{R}_0 \right\} \tag{34}$$

where $\gamma_{\mathcal{A}}, \gamma_{\mathcal{B}}$ are positive scalars, $\mathcal{Q}_0$ and $\mathcal{R}_0$ are empirically imposed positive defined symmetrical matrix.

The focus is to find the $(\gamma_{\mathcal{A}}, \gamma_{\mathcal{B}})$ pair, that defines the maximum uncertainty domain for which the stability and the performances when the nominal command is applied are the same (for the same $(\mathcal{Q}, \mathcal{R})$ pair previously selected).

The matrix pair $(\mathcal{Q}_0, \mathcal{R}_0)$ is obtained by decomposing as follows:

$$\begin{cases} \mathcal{Q} = \mathcal{Q}_0 + \mathcal{Q}_1 \\ \mathcal{R} = \mathcal{R}_0 + \mathcal{R}_1 \end{cases} \tag{35}$$

where the pair $(\mathcal{Q}, \mathcal{R})$ is known from LQR control algorithm. $(\mathcal{Q}_0, \mathcal{R}_0)$ is defined in the Equation (34). $\mathcal{Q}_1$ and $\mathcal{R}_1$ are positively defined symmetrical matrices.

For the nominal optimal state feedback law $u(t)$ and the matrix pair $(\mathcal{Q}_1, \mathcal{R}_1)$, the positive defined symmetric matrix Γ is computed as follows [15]:

$$\Gamma = \mathcal{S}^{-1} \left(\mathcal{Q}_1 + \mathcal{K}_{LQR}^T \mathcal{R}_1 \mathcal{K}_{LQR} \right) \mathcal{S}^{-1} \tag{36}$$

The closed-loop system defined in the Equation (32), with parametric uncertainties, keeps the stability and the optimal performances if the matrix Γ verifies the inequality [15]:

$$\Gamma > (\gamma_{\mathcal{A}} + \gamma_{\mathcal{B}})\, I \tag{37}$$

The control law is derived from the nominal model, adhering to the standard criterion defined in the Equation (27). The selected matrices from the Equation (35) are used to take into account the uncertainties. Therefore, the Inequality (37) propose a rule to obtain the upper bound for the uncertainties, ensuring the closed-loop system remains stable.

3.4.2 Stability margins analysis

In order to determine the extend at which the pair $(\delta\mathcal{A}(t), \delta\mathcal{B}(t))$ can vary by introducing uncertainties in all of the parameters corresponding to the model described by the transfer function in (1), a stability analysis is needed for the closed-loop system defined by $(\mathcal{A}, \mathcal{B}, \mathcal{C}, \mathcal{D})$ and the optimal controller $(\mathcal{K}_{LQR}, \mathcal{Q}, \mathcal{R})$.

When the uncertainties are taken into account for the studied $H_F(s)$, the transfer function in the Equation (1) has the following structure:

$$H_{F_u}(s) = \frac{1}{s} \frac{h_1}{h_2 s^2 + h_3 s + h_4} \tag{38}$$

where $h_1 = h_{1_{init}} + h_{1_{init}} \cdot \left(\frac{h_{p1}}{100}\right)$, $h_2 = h_{2_{init}} + h_{2_{init}} \cdot \left(\frac{h_{p2}}{100}\right)$, $h_3 = h_{3_{init}} + h_{3_{init}} \cdot \left(\frac{h_{p3}}{100}\right)$ and $h_4 = h_{4_{init}} + h_{4_{init}} \cdot \left(\frac{h_{p4}}{100}\right)$, with $h_{1_{init}}$, $h_{2_{init}}$, $h_{3_{init}}$ and $h_{4_{init}}$ - the initial values of the coefficients. Also, h_{p_1}, h_{p_2}, h_{p_3}, h_{p_4} represent the percentage at which every parameter of the transfer function can be varied in order to keep the system stable.

All of the changes in these coefficients will be reflected in $(\mathcal{A}, \mathcal{B}, \mathcal{C})$ and they will become: $(\mathcal{A}_u = A + \Delta A$, $\mathcal{B}_u = B + \Delta B$, $\mathcal{C}_u = C + \Delta C)$. And by studying the robust stability margins of the system, the uncertainties that can be tolerated before the system becomes unstable can be quantified. In the current case, these margins measure how far the parameters h_i can deviate from their nominal values before the closed-loop system poles move into the right half-plane.

The new closed-loop system will have the transfer function:

$$H_{CL_u}(s) = \mathcal{C}_u \left(s\mathbb{I} - (\mathcal{A}_u - \mathcal{B}_u \mathcal{K}_{LQR}) \right)^{-1} \mathcal{B}_u \tag{39}$$

Further, with μ denoted as the inverse of the smallest structured singular value of the matrix corresponding to the closed-loop system. In order to ensure that the system remains stable, the inequality bellow should be valid for any variation in h_i [11]:

$$\mu\left(H_{CL_u}\right) < 1 \tag{40}$$

In practical applications this can be done by adding variations in h_{p_i} percents, which can destabilize them and use numerical optimization to maximize the uncertainties, while checking that the eigenvalues of the closed-loop system matrix $\mathcal{A}_u - \mathcal{B}_u \mathcal{K}_{LQR}$ are still in the negative half-plane.

4 Results and discussions

4.1 Model of the selected variable-oriented photovoltaic system

Since the photovoltaic panel **SPM042152400**, introduced below in the Table 1, has an output power of 215 W [29], a motor with a nominal power of 200 W is used. In addition, to precisely orient the panel towards the sun, the DC motor's electromagnetic coupling constant is $K_m = 0,5 \frac{Nm}{A}$.

Table 1: Datasheet Characteristics: SPM042152400 $215W - 24V$ [29]

Parameter		Value
T_{STC}	Temperature under Standard Test Conditions	$25\,^oC$
G_{STC}	Solar Irradiance under Standard Test Conditions	$1000\,W \cdot m^{-2}$
$U_{oc_{STC}}$	Open-Circuit Voltage	$45.82\,V$
$I_{sc_{STC}}$	Short-Circuit Voltage	$6.3\,A$
$P_{mp_{STC}}$	Nominal Power	$215\,W$
$U_{mp_{STC}}$	Max-power Voltage	$37.4\,V$
$I_{mp_{STC}}$	Max-Power Current	$5.75\,A$
K_i	Temperature coefficient of $I_{sc_{STC}}$	$0.04\,\frac{\%}{^oC}$
K_v	Temperature coefficient of $U_{oc_{STC}}$	$-0.35\,\frac{\%}{^oC}$
Δ_T	Temperature Range	-40^oC to $+\,85^oC$
m_pv	Net weight	$15\,kg$

The selection of the used motor is critical, as it must provide the capability to move the panel. Additionally, the motor's electromagnetic coupling should be suitable for tilting a panel with a weight between $15kg$ and $20kg$. Therefore, a $24V$ DC motor with a rated power of 200 W is selected - ATO-80AS0202-15 [26]. The motor characteristics can be found in the Table 2:

Table 2: The parameters of the ATO-80AS0202-15 DC motor $24V - 200W$ [26]

Parameter		Value
U_e	Armature Nominal Voltage	$24\,V$
ω_{mn}	Rated speed	$1500\,rpm$
U_{max}	Maximum voltage	$32\,V$
I_{max}	Maximum no-load current	$64\,mA$
I_e	Maximum continuous current	$9.4\,A$
$I_{on_{max}}$	Maximum starting current	$39.8\,A$
M_{max}	Maximum torque	$3.8\,Nm$
M_n	Nominal torque	$1.27\,Nm$
R_e	Series resistance	$0.06\,\Omega$
L_e	Armature inductance	$0.28\,mH$
K_m	Motor Torque constant	$0.17\,\frac{Nm}{A}$
K_e	Motor Coupling constant	$0.17\,\frac{Nm}{A}$
D_m	Friction coefficient	$2.5 \cdot 10^{-5}$
J_m	Mechanical inertia	$0.418 \cdot 10^{-3}\,kg \cdot m^2$
Δ_{T_m}	Temperature range	-20^oC to $+\,60^oC$
m_m	Mass of the motor	$2.5kg$
ξ	Efficiency	85%

The Bucharest area is considered in order to compute the average tilt angle of 33.4^o for the panel. In addition, the results of the extended computation depending on the month are given in the Table 3.

Table 3: Tilt angle for the Bucharest area depending on month [28]

Month	Tilt angle [^{o}]
January	43.4
February	38.4
March	33.4
April	28.4
May	23.4
June	18.4
July	23.4
August	28.4
September	33.4
October	38.4
November	43.4
December	48.4

By analyzing the evolution during for a year, it can be deduced that the tilt angle of the panel will not exceed $50^o[0,8727\,rad]$.

Assuming that the photovoltaic panel can be approximately modeled using a gain, based on the Equation (19), the constant from angular momentum to tilt angle is computed as:

$$K_\alpha = \frac{\frac{\Delta\alpha}{\alpha_0}}{\frac{\Delta\omega_m}{\omega_{m0}}} = \frac{\frac{0.8727}{0.6672}}{\frac{523.59}{400.02}} = 0.9995 \tag{41}$$

with α_0 computed as:

$$\alpha_0 = \frac{\omega_{m0} - \omega_{mmin}}{\omega_{mmax} - \omega_{mmin}} \cdot (\alpha_{UI_{max}} - \alpha_{UI_{min}}) + \alpha_{UI_{min}} = \frac{400.02}{523.29} \cdot 0.8727 = 0.6672\ rad \tag{42}$$

A limit power value of $\mathcal{P}_{gen_0} = 150W$ is imposed and obtained transfer function becomes:

$$H_{pv}(s) = K_{pv} = \frac{\frac{\Delta\mathcal{P}_{gen}}{\mathcal{P}_{gen_0}}}{\frac{\Delta\alpha}{\alpha_0}} = \frac{\frac{215}{150}}{\frac{0.8727}{0.6672}} = 1.0958 \tag{43}$$

The power transducer is also modeled through a gain. The $\mathcal{I}_0$ derived from the static characteristic is:

$$\mathcal{I}_0 = \frac{\mathcal{P}_{gen_0} - \mathcal{P}_{gen_{min}}}{\mathcal{P}_{gen_{max}} - \mathcal{P}_{gen_{min}}} \cdot \left(\mathcal{I}_{UI_{max}-\mathcal{I}_{UI_{min}}}\right) + \mathcal{I}_{UI_{min}} = \frac{150}{215} \cdot (20-4) + 4 = 15.1632A \tag{44}$$

The gain of the transducer is computed as:

$$H_T(s) = K_T = \frac{\frac{\Delta\mathcal{I}}{\mathcal{I}_0}}{\frac{\Delta\mathcal{P}_{gen}}{\mathcal{P}_{gen_0}}} = \frac{\frac{16}{15.1632}}{\frac{215}{150}} = 0.7362 \tag{45}$$

Taking into account the already computed models, the entire photovoltaic system's transfer function is defined by connecting all the sub-systems in series [5]:

$$H_F(s) = H_m \cdot H_{pv}(s) \cdot H_T(s) = \frac{1}{s} \cdot \frac{137.09}{0.117 \cdot 10^{-3} \cdot s^2 + 0.02509 \cdot s + 28.9} \tag{46}$$

To derive the state-space representation and fully characterize the system's behavior, three state variables are necessary. Using the transfer function defined in the Equation (1), the model can be realized as a quadruple $(\mathcal{A}, \mathcal{B}, \mathcal{C}, \mathcal{D})$, where:

$$\mathcal{A} = \begin{bmatrix} -214.44 & -482.4386 & 0 \\ 512 & 0 & 0 \\ 0 & 1 & 0 \end{bmatrix} \qquad \mathcal{B} = \begin{bmatrix} 64 \\ 0 \\ 0 \end{bmatrix}$$
$$\mathcal{C} = \begin{bmatrix} 0 & 0 & 35.7577 \end{bmatrix} \qquad \mathcal{D} = \begin{bmatrix} 0 \end{bmatrix} \tag{47}$$

The controllability matrix $\mathbf{C}_F = [\mathcal{B}\ \mathcal{A}\mathcal{B}\ \mathcal{A}^2\mathcal{B}]$ [25] has a rank of 3, which is identical to $rank(\mathcal{A}) = 3$, indicating that there are 3 independent variables. This is also reflected in the degree of the transfer function.

The observability matrix $\mathbf{O}_F = \begin{bmatrix} \mathcal{C} \\ \mathcal{C}\mathcal{A} \\ \mathcal{C}\mathcal{A}^2 \end{bmatrix}$ [25] also has a rank of 3. Therefore, the pair $(\mathcal{B}, \mathcal{A})$ is controllable and the pair $(\mathcal{C}, \mathcal{A})$ is observable. Consequently, the realization is minimal.

Therefore, a state feedback control law can be computed, or a regulator with an integrated state estimator can be designed.

4.2 Optimal control designed for the photovoltaic system

To compute the stabilizing state-feedback control law in the Equation (27), the matrices pair $(\mathcal{Q}, \mathcal{R})$ are empirically chosen based on the system's limitations, where $\mathcal{Q}\ in\mathbb{R}^{3\times3}$ and $\mathcal{R} \in \mathbb{R}$.

$\mathcal{R}$ is a unit cost in this case, as more weight on the control means there will not be a significant improvement for what's designed via control. The positive definite diagonal matrix $\mathcal{Q}$ is given by:

$$\mathcal{Q} = \begin{bmatrix} 5.73 & 0 & 0 \\ 0 & 1.23 & 0 \\ 0 & 0 & 1423.92 \end{bmatrix} \quad \mathcal{R} = \begin{bmatrix} 1 \end{bmatrix} \tag{48}$$

In this case, the resulted $\mathcal{K}_{LQR}$ computed based on the Equation (28) is:

$$\mathcal{K}_{LQR} = \begin{bmatrix} 0.9998 & 0.1231 & 37.7349 \end{bmatrix} \tag{49}$$

Therefore, the closed-loop system is stable, because the poles $-137.22+480.51j$, $-137.72-480.51j$ and -3.98 are placed in the left half-plane. The complex-conjugate pair suggests that the system has oscillatory components, but the large negative real part indicates that these oscillations will decay very quickly. The real eigenvalue defines the long-term behavior of systems, as the effects of the other eigenvalues will decay much faster. The simulated result is represented in the Figure 5:

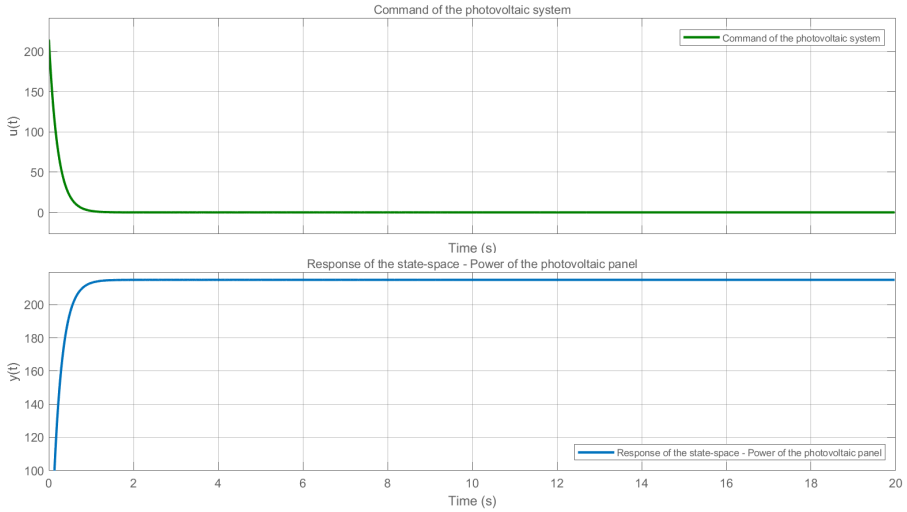

Figure 5: The response of the closed-loop system using LQR control law

The performances of this controller can be summarized as zero overshot when reaching the reference power of $215\,W$, following it with zero steady-state error and a transient time of 0.629 seconds.

4.3 Evaluation of the maximum uncertainty region - Parametric uncertainties & Stability Margins of the Photovoltaic System

When the uncertainties are taken into account, the transfer function (1) has the following structure based on (38):

$$H_{F_u}(s) = \frac{137.09\left(1 \pm \frac{h_{p_1}}{100}\right)}{\left(0.117 \cdot 10^{-3}\left(1 \pm \frac{h_{p_2}}{100}\right)\right)s^3 + \left(0.02509\left(1 \pm \frac{h_{p_3}}{100}\right)\right)s^2 + \left(28.9\left(1 \pm \frac{h_{p_4}}{100}\right)\right)s} \tag{50}$$

Applying the defined methodology for the system, it was identified that h_1 can vary by $h_{p_1} = 91.06\%$, h_2 can vary by $h_{p_2} = 72.22\%$, h_3 can vary by $h_{p_3} = 65.94\%$ and h_4 can vary by up to $h_{p_4} = 78.5\%$. These values indicate that the system can have large variations and it will be maintained stable by the same $\mathcal{K}_{LQR}$. The highest variations can be added to the numerator of the transfer function, and that shows that even at high deviations produced by the solar irradiance, temperature, partial shading or other environmental conditions, the system will keep the stability margins.

The values for the output corresponding to the margins found by applying this method on the closed-loop system are represented in the Figure 6:

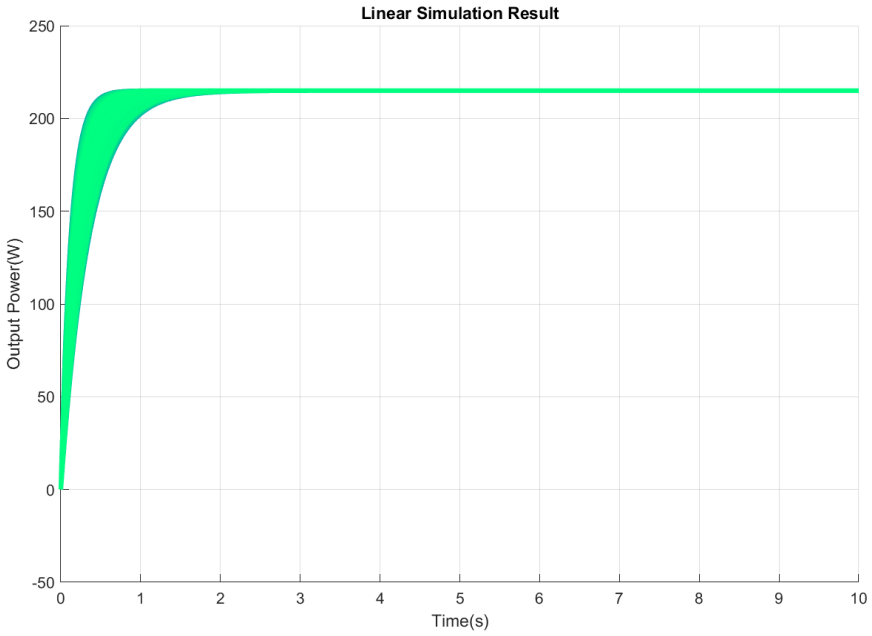

Figure 6: The output of the closed-loop system, that keeps the system's stability

The matrix pair $(\mathcal{Q}_0, \mathcal{R}_0)$ from (35) were chosen simetric and positive defined as:

$$\begin{cases} \mathcal{Q}_0 = \mathcal{C}^T\mathcal{C} + \mathbb{I} \\ \mathcal{R}_0 = [0.01] \end{cases} \tag{51}$$

Choosing $\mathcal{Q}_0$ will ensure that all states are penalized, even though $\mathcal{C}$ has some elements equal to zero. Also, it prevents ignoring any state in the cost function, providing stability and performances for the entire system. Moreover, it will penalize heavier the state with high impact on the output, in order to align the control effort to the desired output performances. Additionally, the identity matrix enhances numeric stability, by ensuring that the matrix is positive definite, leading to robust and stable solutions. Furthermore, this selection is a useful approach for implementation of the controller, because of simplifying the design process by leveraging the known system matrices $\mathcal{C}$ and the identity matrix $\mathbb{I}$. This can make a practical choice in applications for the ease of implementation.

The drawback of this $\mathcal{Q}_0$ can be that adding the bias $\mathbb{I}$, could lead to excessive control actions, because the matrix can be not appropriately scaled, or this might lead to actuator saturation. But, this is why the identity matrix was the choice, because it has values of ones, which are significantly lower than the term resulted from $\mathcal{C}^T\mathcal{C}$, implying that the control effort for the other states is minimal, considering its benefits in the numerical properties of the matrix $\mathcal{Q}_0$, system control, robustness and performances as in [22].

The defined margins will lead to an analysis consisting of two case studies: one in which all the parameters are varied up with the defined percentages for the margins and one in which they are varied down. This is because the worse case scenarios will be studied to define the bounds between which γ_A and γ_B can vary.

4.3.1 Case 1 - The parameters are varied towards the upper margins

Since the parameters of the transfer function are set up with the specified percentages, the values for the variations $(\Delta\mathcal{A}_+, \Delta\mathcal{B}_+)$ can be computed as:

$$\Delta\mathcal{A}_+ = \begin{bmatrix} 7.8153 & -17.5921 & 0 \\ 0 & 0 & 0 \\ 0 & 0 & 0 \end{bmatrix} \quad \Delta\mathcal{B}_+ = \begin{bmatrix} 0 \\ 0 \\ 0 \end{bmatrix} \tag{52}$$

The resulted solution of the Riccati equation from (29) is:

$$S = \begin{bmatrix} 0.0156 & 0.0019 & 0.5896 \\ 0.0019 & 0.0146 & 0.3206 \\ 0.5896 & 0.3206 & 289.095 \end{bmatrix} \tag{53}$$

With this values, the matrix Γ from (36) is computed as:

$$\Gamma = \begin{bmatrix} 27174.996 & -2157.61 & -44.827 \\ -2157.61 & 1332.96 & 2.889 \\ -44.827 & 2.889 & 0.0901 \end{bmatrix} \tag{54}$$

For the defined margins, the values of γ_{A_+} and γ_{B_+} are calculated taking into account the relation (37) and the uncertainty domain D_u.

$$\begin{cases} \gamma_{A_+} = 370.5615 \\ \gamma_{B_+} = 0 \end{cases} \tag{55}$$

In this case, the value of γ_{B_+} is zero, because of the fact that the $\mathcal{B}$ has only the first element not null and when adding the maximum variations that will not destabilize the system. Also, the new matrices, that define the system with uncertainties are:

$$\mathcal{A}_{u_+} = \begin{bmatrix} -206.6247 & -500.0307 & 0 \\ 512 & 0 & 0 \\ 0 & 1 & 0 \end{bmatrix} \qquad \mathcal{B}_{u_+} = \mathcal{B} = \begin{bmatrix} 64 \\ 0 \\ 0 \end{bmatrix}$$
$$\mathcal{C}_{u_+} = \begin{bmatrix} 0 & 0 & 39.6694 \end{bmatrix} \qquad \mathcal{D}_{u_+} = \mathcal{D} = \begin{bmatrix} 0 \end{bmatrix} \tag{56}$$

The new system representation in the state space was proved to have similar performances, for the same $\mathcal{K}_{LQR} = \begin{bmatrix} 0.9998 & 0.1231 & 37.7349 \end{bmatrix}$, in simulation and the result from the Figure 7.

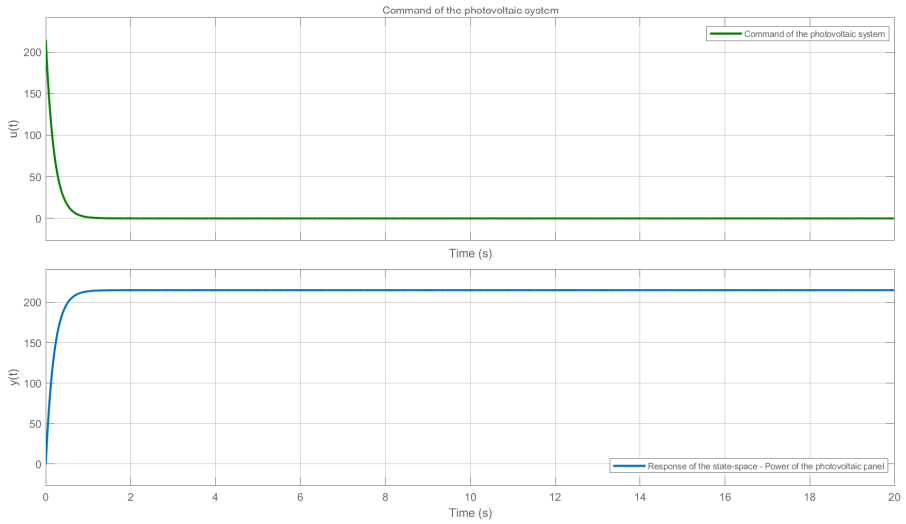

Figure 7: The output of the closed-loop system, for the maximum upper uncertainties

The transient time for this case is 0.588 sec, which is faster than 0.629 sec for the initial system. This is because the matrix $\mathcal{A}_{u_+}$ and $\mathcal{C}_{u_+}$, define higher gains and introduce a faster dynamic for the system, for which the controller keeps zero overshoot and helps the system reach the reference, by applying a command with values in a similar range as for the initial system.

4.3.2 Case 2 - The parameters are varied towards the lower margins

In this case, the parameters of the transfer function are all varied down with the defined percentages, thus the computed values for $(\Delta\mathcal{A}_-, \Delta\mathcal{B}_-)$ are:

$$\Delta\mathcal{A}_- = \begin{bmatrix} -48.4822 & 109.0610 & 0 \\ 0 & 0 & 0 \\ 0 & 0 & 0 \end{bmatrix} \quad \Delta\mathcal{B}_- = \begin{bmatrix} -32 \\ 0 \\ 0 \end{bmatrix} \tag{57}$$

Both the Riccati equation solution S and the matrix Γ have the same values. But, the domain D_u is now changed, therefore the values of γ_{A_-} and γ_{B_-} are computed as:

$$\begin{cases} \gamma_{A_-} = 14244.8162 \\ \gamma_{B_-} = 3200 \end{cases} \tag{58}$$

The new matrices defining the state-space representation of the uncertain system for this case have the values:

$$\mathcal{A}_{u_-} = \begin{bmatrix} -262.9222 & -373.3776 & 0 \\ 512 & 0 & 0 \\ 0 & 1 & 0 \end{bmatrix} \qquad \mathcal{B}_{u_-} = \begin{bmatrix} 32 \\ 0 \\ 0 \end{bmatrix}$$
$$\mathcal{C}_{u_-} = \begin{bmatrix} 0 & 0 & 23.0147 \end{bmatrix} \qquad \mathcal{D}_{u_-} = \mathcal{D} = \begin{bmatrix} 0 \end{bmatrix} \tag{59}$$

The system defined with these inferior margins for the parameters, also proves that the same $\mathcal{K}_{LQR}$ keeps stability and the response has zero overshoot as can be visualized in the Figure 8.

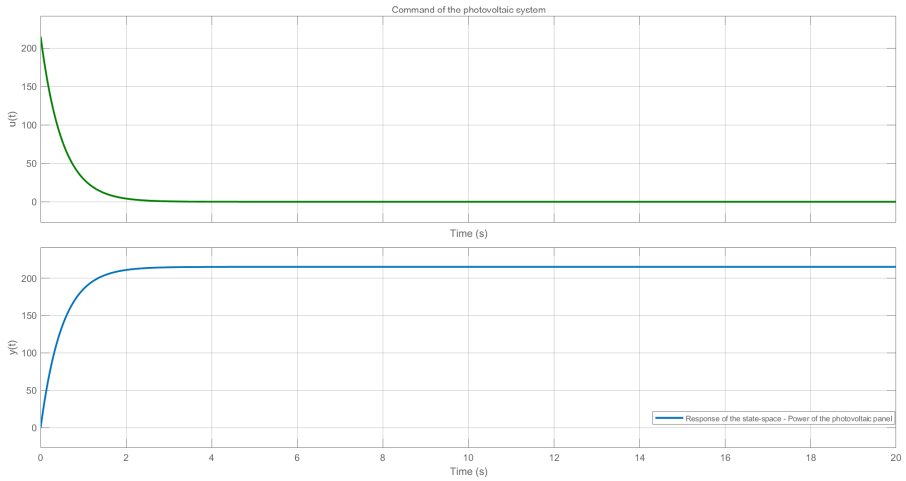

Figure 8: The output of the closed-loop system, for the maximum lower uncertainties

For this case, the transient time in which the same reference is reached is 1.518 seconds. It is clear that the system defined for the lower margins of the parameters has much slower dynamics, which can be seen from the matrix defining this state-space realization of the system. Also, this is a realistic case, where both the motor and the photovoltaic panel slows down their dynamics, because of the aging of their components and environmental conditions.

5 Conclusion

The current paper has brought to light a robust LQR controller for a variable-oriented photovoltaic system, that aims to deliver and maintain at the end customer a maximum power of 215 W. The designed controller was proved to keep high performances for consistent variations of the system's model. This will be an advantage, when it will be implemented on a real world photovoltaic application, because it will act properly for changes in irradiance, temperature, shading, other environmental factors or a limited degradation of some parts of the system over time.

A robust LQR controller designed for the photovoltaic system with variable tilt angle enhances energy efficiency. By optimizing the tilt angle in real-time, the system maximizes the captured solar energy during the daytime and across different seasons and weather conditions. This adaptability is crucial for maintaining high energy output in diverse and unpredictable climates.

The controller enhances the overall stability of the solar tracking system. It was shown in the current work, that it keeps oscillations to zero and minimizes disturbances, leading to smoother the operation and reduced overloading of mechanical components.

While the initial investment in adding a DC-DC motor to the photovoltaic system and in implementing a LQR controller may come with some additional costs, long-term benefits include increased energy production and reduced maintenance costs. This makes the defined system a cost-effective solution for sustainable large-scale energy production, making it also suitable for fields of photovoltaic panels. Moreover, this system can be easily scaled and integrated into existing solar power infrastructures.

Maximizing the efficacy of solar energy captured, the system contributes to reduce fossil fuels and decreases greenhouse gas emissions. This supports the general efforts to reduce the climate change and to boost the renewable energy resources.

The success of the designed LQR controller in managing variable tilt angles and relatively high variations in the model of the system, opens avenues for further research. Future developments could focus on implementing the controller on a real-time application, enhancing the control algorithms, integrating machine learning techniques to determine the Q and R matrix or to learn from the seasonal trends and vary between different controllers, and exploring new materials for improved panel efficiency.

The main drawback of the strategy was that the design required solving a Riccati equation, which can add some computational complexity. In the current case, the order of the involved matrix was three, but the complexity will increase with the number of states. Another drawback is that the LQR controller performances are hardly linked to the mathematical accuracy of the modeled system and to the strategy of selecting $\mathcal{Q}$ and $\mathcal{R}$ matrices. Any differences between the model and the real system may result in instability or suboptimal performance. In addition, the selection of the pair $(\mathcal{Q}, \mathcal{R})$ depends on the system's limitations, and in the majority of cases the proper way to choose them is empirically.

Author contributions

The authors contributed equally to this work.

Conflict of interest

The authors declare no conflict of interest.

References

[1] Abut, T. (2016). Modeling and optimal control of a DC motor, *Int. J. Eng. Trends Technol*, 32(3), 146–150, 2016.

[2] Alomar, O.R; Ali, O. M.; Ali, B. M.; Qader, V. S.; Ali, O. M. (2023). Energy, exergy, economical and environmental analysis of photovoltaic solar panel for fixed, single and dual axis tracking systems: An experimental and theoretical study, *Case Studies in Thermal Engineering*, Elsevier, 51, 103635, 2023.

[3] Anbarasi, M. P.; Kanthalakshmi, S. (2016). Linear quadratic optimal control of solar photovoltaic system: An experimental validation, *Journal of Renewable and Sustainable Energy*, AIP Publishing 8(5), 2016.

[4] Assouline, D.; Mohajeri, N.; Scartezzini, J.L. (2017). Quantifying rooftop photovoltaic solar energy potential: A machine learning approach, *Solar Energy*, Elsevier, 141, 278–296, 2017.

[5] Bancila, D.M.; Popescu, D.; Colbu, S.C.; Megard, A.; Blanchard, M. (2022). Optimal control for solar tracking systems, *Proceedings of the 2022 26th International Conference on System Theory, Control and Computing (ICSTCC)*, IEEE 509–514, 2022.

[6] Boubaker, O. (2022). A comprehensive review and classified comparison of MPPT algorithms in PV systems, *Energy Systems*, Springer 13(2), 281–320 ,2022.

[7] Boubaker, O. (2023). MPPT techniques for photovoltaic systems: a systematic review in current trends and recent advances in artificial intelligence, *Discover Energy*, Springer 3(1), 2023.

[8] Brogan, W.L. (1991). *Modern control theory*, Prentice-Hall, 1991.

[9] Calabrò, E. (2009). Determining optimum tilt angles of photovoltaic panels at typical north-tropical latitudes, *Journal of renewable and sustainable energy*, AIP Publishing 1(3), 2009.

[10] Hassan, Q; Abbas, M. K,; Abdulateef, A. M.; Abdulateef, J.; Mohamad, A. (2021). Assessment the potential solar energy with the models for optimum tilt angles of maximum solar irradiance for Iraq, *Case Studies in Chemical and Environmental Engineering*, Elsevier, 4, 100140, 2021.

[11] Kashyap, M.; Lessard, L. (2023). Guaranteed stability margins for decentralized linear quadratic regulators *IEEE Control Systems Letters*, IEEE 7, 1778–1782, 2023.

[12] Li, D.H.W.; Lam, T.N.T; Chu, V.W.C (2008). Relationship between the total solar radiation on tilted surfaces and the sunshine hours in Hong Kong, In *Solar energy*, Elsevier, 82(12), 1220–1228, 2008.

[13] Liu, J.; Qu, Q.; Yang, H.; Zhang, J.; Liu, Z. (2024). Deep learning-based intelligent fault diagnosis for power distribution networks, *International Journal of Computers Communications & Control*, 19(4), 2024.

[14] Mazumdar, D.; Sain, C; Biswas, P.K.; Sanjeevikumar, P. and Khan, B. (2024). Overview of solar photovoltaic MPPT methods: a state of the art on conventional and artificial intelligence control techniques, *International Transactions on Electrical Energy Systems*, 2024(1), 8363342, 2024.

[15] Mone, M.A.; Diop, S.; Popescu, D.(2021). Evaluating the maximum domain of parameter model uncertainties in the combustion of a Diesel engine, *Proceedings of the 2021 25th International Conference on System Theory, Control and Computing (ICSTCC)*, IEEE 12–17, 2021.

[16] Montoya, G.; Lozano-Garzón, C.; Paternina-Arboleda, C.; Donoso, Y. (2025). A Mathematical Optimization Approach for Prioritized Services in IoT Networks for Energy-constrained Smart Cities, *International Journal of Computers Communications & Control*, 20(1), 2025.

[17] Mukhatov, A.; Thao, N. G. M.; Do, T. D. (2022). Linear quadratic regulator and fuzzy control for grid-connected photovoltaic systems, *Energies*, MDPI 15(4), 1286, 2022.

[18] Oaxaca-Adams, G; Villafuerte-Segura, R.; Aguirre-Hernández, B. (2024). On Hurwitz stability for families of polynomials, *International Journal of Robust and Nonlinear Control*, 34(7), 4576–4594, 2024.

[19] Rahdan, P.; Zeyen, E.; Gallego-Castillo, C.; Victoria, M. (2024). Distributed photovoltaics provides key benefits for a highly renewable European energy system, *Applied Energy*, Elsevier, 360, 122721, 2024.

[20] Ritchie, H.; Roser, M.; Rosado, P. (2020). Renewable Energy, *Our World in Data*, [Online]. Available: https://ourworldindata.org/renewable-energy/, Accesed on 08 July 2024 .

[21] Rowell, D. (2002). State-space representation of LTI systems, *URL: http://web. mit. edu/2.14/www/Handouts/StateSpace. pdf*, 1–18, 2002.

[22] Sadraddini, S.; Tedrake, R. (2020). Robust output feedback control with guaranteed constraint satisfaction *Proceedings of the 23rd International Conference on Hybrid Systems: Computation and Control* 1–10, 2020.

[23] Sarailoo, M.; Akhlaghi, S.; Rezaeiahari, M.; Sangrody, H. (2017). Residential solar panel performance improvement based on optimal intervals and optimal tilt angle, *2017 IEEE Power & Energy Society General Meeting*, IEEE, 1–5, 2017.

[24] Sharma, D.; Jalil, M. F.; Ansari, M. S.; Bansal, R.C. (2024). A Review of Maximum Power Point Tracking (MPPT) Techniques for Photovoltaic Array Under Mismatch Conditions, *Photovoltaic Systems Technology*, 85–102, 2024.

[25] Terrell, W.J. (1999). Some fundamental control theory I: controllability, observability, and duality, *The American Mathematical Monthly*, Taylor & Francis 106(8), 705–719, 1999.

[26] [Online]. Available: https://www.ato.com/200w-dc-servo-motor, Accessed on 15 August 2024.

[27] [Online]. Available: https://ec.europa.eu/eurostat/statistics-explained/index.php?title= Renewable_energy_statistics\#Share_of_renewable_energy_more_than_doubled_between_2004_and_2022, Accesed on 08 July 2024.

[28] [Online]. Available: https://solarmentors.com/solar-panel-tilt-angle-calculator/, Accessed on 15 August 2024.

[29] [Online]. Available: https://www.victronenergy.com/upload/documents/Datasheet-BlueSolar-Monocrystalline-Panels-EN-.pdf, Accessed on 15 August 2024.

Journal's webpage: http://univagora.ro/jour/index.php/ijccc/

This journal is a member of, and subscribes to the principles of,
the Committee on Publication Ethics (COPE).
https://publicationethics.org/members/international-journal-computers-communications-and-control

Cite this paper as:

Bancila, D.; Colbu, S.; Popescu, D. (2025). Evaluating the Maximum Region for Parametric Model Uncertainties in Variable-Oriented Photovoltaic Systems, *International Journal of Computers Communications & Control*, 20(5), 6829, 2025.
https://doi.org/10.15837/ijccc.2025.5.6829